

Probing FtsZ and Tubulin with C8-Substituted GTP Analogs Reveals Differences in Their Nucleotide Binding Sites

Tilman Lippchen,¹ Victorine A. Pinas,¹ Aloysius F. Hartog,¹ Gerrit-Jan Koomen,¹ Claudia Schaffner-Barbero,² José Manuel Andreu,² Daniel Trambaiolo,³ Jan Löwe,³ Aurélie Juhem,^{4,6,7} Andrei V. Popov,^{4,6,7} and Tanneke den Blaauwen^{5,*}

¹Van 't Hoff Institute for Molecular Sciences, Bioorganic Chemistry, University of Amsterdam, Nieuwe Achtergracht 129, 1018 WS Amsterdam, The Netherlands

²Centro de Investigaciones Biológicas, CSIC, Ramiro de Maeztu 9, 28040 Madrid, Spain

³MRC Laboratory of Molecular Biology, Hills Road, Cambridge CB2 2QH, United Kingdom

⁴Laboratoire du cytosquelette, Inserm Unité 366, DRDC/CS, CEA-Grenoble, 17 rue des Martyrs, 38054 Grenoble, Cedex 9, France

⁵Swammerdam Institute for Life Sciences, Molecular Cytology, University of Amsterdam, Kruislaan 316, 1098 SM Amsterdam, The Netherlands

⁶Present address: Inserm Unité 836, 38043 Grenoble, France.

⁷Present address: Université Joseph Fourier, Institut des Neurosciences, 38043 Grenoble, France.

*Correspondence: blaauwen@science.uva.nl

DOI 10.1016/j.chembiol.2007.12.013

SUMMARY

The cytoskeletal proteins, FtsZ and tubulin, play a pivotal role in prokaryotic cell division and eukaryotic chromosome segregation, respectively. Selective inhibitors of the GTP-dependent polymerization of FtsZ could constitute a new class of antibiotics, while several inhibitors of tubulin are widely used in antiproliferative therapy. In this work, we set out to identify selective inhibitors of FtsZ based on the structure of its natural ligand, GTP. We found that GTP analogs with small hydrophobic substituents at C8 of the nucleobase efficiently inhibit FtsZ polymerization, whereas they have an opposite effect on the polymerization of tubulin. The inhibitory activity of the GTP analogs on FtsZ polymerization allowed us to crystallize FtsZ in complex with C8-morpholino-GTP, revealing the binding mode of a GTP derivative containing a nonmodified triphosphate chain.

INTRODUCTION

The essential cytoskeletal proteins, FtsZ and tubulin, play a central role in the organization of prokaryotic and eukaryotic cells, respectively. In vivo, GTP-induced polymerization of FtsZ into a macromolecular structure termed the Z ring is a key event in bacterial cell division (reviewed by Huang et al. [2007] and Michie and Löwe [2006]). Agents interfering with FtsZ polymerization potentially inhibit septum formation and cell division, and may be developed into a promising class of novel antibiotics with low potential for cross resistance to currently available antibacterial agents (Huang et al., 2006; Paradis-Bleau et al., 2007; for a recent review on small-molecule FtsZ inhibitors, see Vollmer, 2006). Similar to FtsZ, GTP induces polymerization of α , β -tubulin heterodimers into "sheets," which progressively close themselves

into hollow cylindrical structures known as microtubules. In mitosis, they form the mitotic spindle, required for proper chromosome segregation (reviewed by Nogales and Wang [2006a] and Nogales and Wang [2006b]). As such, they are indispensable for eukaryotic cell proliferation and form an important target for anticancer drugs.

Although FtsZ shows only weak sequence identity to the eukaryotic tubulins (Erickson, 1995), it is generally considered a true prokaryotic homolog of tubulin because of the similar three-dimensional structures of the two proteins and their conserved longitudinal protofilament contacts (Löwe and Amos, 1998; Löwe et al., 2001; Oliva et al., 2004). In vitro, GTP induces assembly of FtsZ into linear protofilaments, which may laterally associate to form protofilament bundles. FtsZ polymerization activates its GTPase activity, leading to depolymerization upon depletion of GTP (Mukherjee and Lutkenhaus, 1998). While activation of the GTPase function of FtsZ requires oligomerization, polymerization of FtsZ is not dependent on GTP hydrolysis (Löwe and Amos, 2000; Lu et al., 2000). The published crystal structure of an FtsZ dimer provides detailed structural insights into the longitudinal contacts within the protofilaments and the GTPase active site (Oliva et al., 2004), confirming earlier biochemical evidence that the active site is formed by association of monomers (Scheffers et al., 2002).

One of the major differences between FtsZ and tubulin is in their GTPase reaction kinetics. In the case of tubulin, assembly and GTP hydrolysis are closely coupled and nucleotide exchange within the polymer is negligible, resulting in polymers containing mainly GDP and a stabilizing cap of GTP-bound tubulin subunits at the fast-growing (+) end. GTP hydrolysis introduces considerable strain into the microtubule structure, since the GDP-bound tubulin protofilaments, which naturally prefer a more outward-curved conformation, are forced to remain straight within the microtubule due to the lateral contacts with neighboring protofilaments. Random loss and restoration of the GTP-tubulin cap is thought to cause the observed stochastic and reversible transitions between growth and rapid shrinkage of individual

microtubules known as “dynamic instability” (reviewed by Nogales and Wang [2006b]). In contrast, several studies suggest that FtsZ polymers allow comparatively free nucleotide exchange within the polymers (Huecas and Andreu, 2003; Mingorance et al., 2001; Romberg and Mitchison, 2004), rendering GTP hydrolysis the major rate-limiting step in GTP turnover in FtsZ polymers (Romberg and Mitchison, 2004). The dissimilar reaction kinetics of the two proteins are reflected in their respective protofilament structures, which reveal major differences in the solvent accessibility of their nucleotide binding pockets (Oliva et al., 2004). In tubulin protofilaments, the nucleotides are completely occluded by the protein, and nucleotide exchange may only occur after disassembly. In the FtsZ dimer, by contrast, the nucleotide binding pocket is open enough to allow free diffusion of GTP into the intact protofilament.

In the search for new classes of antibiotics, much effort has recently been directed toward the identification of compounds interfering with FtsZ polymerization. Nucleotide derivatives, however, have not yet gained much attention. Apart from early reports on the nucleoside triphosphate specificity of FtsZ (Mukherjee et al., 1993), investigations have been limited to the effects of the nonhydrolyzable GTP analogs, GTP- γ -S (Scheffers et al., 2000), GMPCPP, and GMPPCP (Löwe and Amos, 2000; Lu et al., 2000). We recently discovered that 8-bromoguanosine 5'-triphosphate (BrGTP) inhibits both the polymerization of FtsZ and its GTPase activity (Läppchen et al., 2005). In this article, we describe the preparation of a structurally diverse series of C8-substituted GTP analogs, the investigation of their effects on both FtsZ and tubulin, and the characterization of their binding to FtsZ by protein crystallography. While all GTP analogs were found to inhibit FtsZ polymerization, some of them potently induced tubulin assembly. We conclude that these opposing effects of C8-substituted GTP analogs on FtsZ and tubulin reflect differences in their nucleotide binding sites. Our results open the way for the design of selective GTP-based inhibitors of FtsZ polymerization, which may give rise to a new generation of antibiotics.

RESULTS AND DISCUSSION

Chemical Synthesis

Starting from guanosine, the GTP analogs were prepared by first introducing the C8-substituents and subsequently the 5'-triphosphate chain. 8-Methylguanosine (**1a**, Figure 1A) (Maeda et al., 1974) and 8-*t*-butylguanosine (**2a**, Figure 1A; Pless et al., 1978) were obtained by free radical alkylation of guanosine in acidic aqueous solution. Depending on the type of halogen, different synthetic approaches were required for the halogenation of guanosine. Iodination was achieved with *N*-iodosuccinimide and catalytic amounts of *n*-butyl disulfide in DMSO (Lipkin et al., 1963), chlorination with *m*-chloroperbenzoic acid and HCl in *N,N*-dimethylacetamide (Ryu and MacCoss, 1981), and bromination with molecular bromine in water (Long et al., 1968). Nucleophilic aromatic substitution of 8-bromoguanosine (**5a**, Figure 1A) provided access to 8-methoxyguanosine (**6a**, Figure 1A) and a series of 8-alkylaminoguanosines (**7a**, **8a**, and **9a**, Figure 1A), which were obtained in good yields simply by refluxing 8-bromoguanosine in the corresponding amine. 8-Phenylguanosine (**10a**, Figure 1A) was prepared by Suzuki arylation of 8-bromoguanosine, as previously described (Western et al., 2003).

The C8-substituted guanosines were subsequently converted to the corresponding 5'-triphosphates by a convenient one-pot, three-step phosphorylation protocol (Läppchen et al., 2005). The method is based on the 5'-phosphorylation of unprotected nucleosides with POCl₃ in anhydrous trimethyl phosphate followed by reaction of the intermediate nucleoside dichlorophosphates with bis(tri-*n*-butylammonium) pyrophosphate in dry DMF and quenching with aqueous triethylammonium bicarbonate buffer (Figure 1B).

Functional Inhibition of FtsZ by C8-Substituted GTP Analogs

Preliminary studies revealed that all GTP analogs under investigation did not support FtsZ polymerization themselves, but instead interfered with the GTP-dependent polymerization of FtsZ. To obtain quantitative data on the potency of the GTP-analogs toward inhibition of FtsZ polymerization, we investigated the GTP-induced polymerization of FtsZ from *Escherichia coli* in the presence of different concentrations of analogs, ranging from 0 to 360 μ M. Representative results for MeOGTP (the most potent analog) are depicted in Figure 2. IC₅₀ values for polymerization (Table 1) were estimated from semi-log plots of the percentage of polymerization (relative to the control without analogs) versus the concentration of GTP analogs as described for BrGTP (Läppchen et al., 2005). For MeOGTP, the IC₅₀ for polymerization was about 10 μ M in the presence of 60 μ M GTP (Figure 2A), approximately 20 μ M when employing 120 μ M GTP (Figure 2B), and roughly 30 μ M for 180 μ M GTP (data not shown). Hence, similar to BrGTP, the IC₅₀s obtained for MeOGTP depend on the MeOGTP:GTP ratio, suggesting a competitive type of inhibition.

After performing the polymerization experiments, the nucleotide composition of the assay mixtures was determined by HPLC analysis. In general, hydrolysis of GTP analogs was less than 3% (i.e., they were not substrates for FtsZ). The endpoint GTP hydrolysis data (Figure 2C, Table 1; see also Tables S1–S9 in the Supplemental Data available with this article) obtained after the polymerization assays in the presence of 60 μ M GTP analogs (1:1 molar ratio of GTP analog to GTP) clearly indicates that the potency of the GTP analogs toward inhibition of FtsZ polymerization and their ability to inhibit FtsZ GTPase activity are closely related.

The endpoint GTP hydrolysis data, although a rough first estimation, do not provide detailed information on the potency of the analogs toward inhibition of FtsZ GTPase activity. Therefore, we set out to determine the IC₅₀ values for GTPase activity by a real-time fluorescence assay for phosphate release, which allows direct monitoring of GTP hydrolysis and the calculation of the initial rates measured under essentially the same conditions as those employed in the polymerization studies (Figure S1). The results were used for the construction of log dose-response curves, as illustrated in Figure 2D. Nonlinear regression analysis of the initial rates of GTP hydrolysis in the presence of various concentrations of GTP analogs allowed the determination of their IC₅₀ (Table 1). The most potent GTP analog in the series, MeOGTP, with an IC₅₀(GTPase) of 15 μ M, was about four times more active than BrGTP, while NMePipGTP was on the other side of the range, with an IC₅₀(GTPase) of approximately 300 μ M. The IC₅₀s for GTPase activity generally matched well with those obtained for FtsZ polymerization, although the former

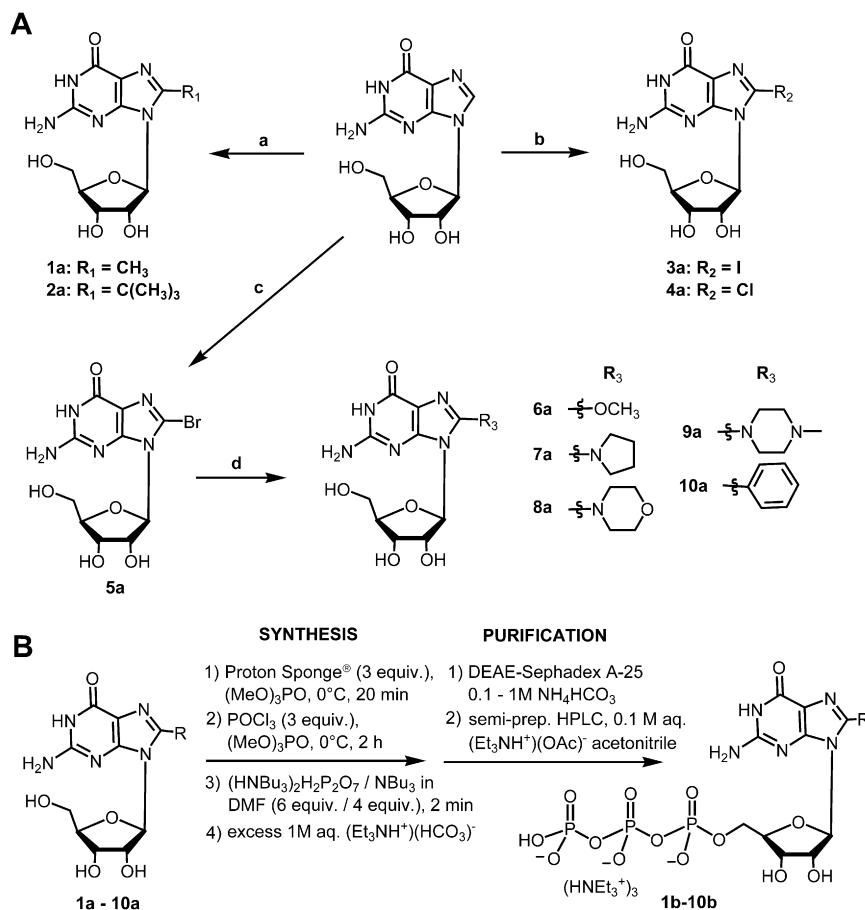


Figure 1. Synthesis of C8-Substituted GTP Analogs

(A) Preparation of C8-substituted guanosine derivatives. Reagents and conditions: (a) $\text{FeSO}_4 \times 7\text{H}_2\text{O}$, $t\text{-BuOOH}$, aq. H_2SO_4 , 30% (**1a**); pivalaldehyde, $\text{Fe}(\text{NH}_4)_2(\text{SO}_4)_2 \times 6\text{H}_2\text{O}$, $\text{K}_2\text{S}_2\text{O}_8$, $\text{H}_2\text{O-HOAc-H}_2\text{SO}_4$, 21% (**2a**); (b) *N*-iodosuccinimide, *n*-butyl disulfide, DMSO, 18 h, 47% (**3a**); MCPBA, HCl, DMA (**4a**); (c) $\text{Br}_2\text{-H}_2\text{O}$, 85% (**5a**); (d) $\text{NaOCH}_3\text{-MeOH}$, DMSO, 65°C , 18 hr, 91% (**6a**); pyrrolidine, reflux, 18 hr, 74% (**7a**); morpholine, reflux, 18 hr, 78% (**8a**); *N*-methylpiperazine, reflux, 18 hr, 69% (**9a**); phenylboronic acid, Na_2CO_3 , TPPTS, $\text{Pd}(\text{OAc})_2$, $\text{H}_2\text{O-CH}_3\text{CN}$ 2:1, 80°C , 3 hr, 75% (**10a**). (B) 5'-Triphosphorylation of the C8-substituted guanosines to the corresponding GTP analogs.

Sterimol B1 parameters (Figures 2F and 2G). Substituents with lower B1 values experience less sterical hindrance with the ribose moiety, and favor glycosidic torsion angles in the *anti*-range (like GTP), while larger substituents favor *syn*-type conformations. As all GTP analogs studied in crystal structures of FtsZ thus far have been found to bind in the *anti* conformation (Oliva et al., 2007), including the very bulky MorphGTP (see below), the lower affinity of GTP analogs with sterically more demanding C8-substituents could partly be attributed to the fact that binding would have to pull from

were consistently about 20%–60% higher. Similar to our results in the presence of BrGTP, the other GTP analogs also presumably gave rise to a large fraction of short FtsZ filaments, which still possessed full GTPase activity, but at the same time had a significantly reduced level of light scattering (Läppchen et al., 2005).

In conclusion, we have designed a series of C8-substituted GTP analogs, which proved to be potent competitive inhibitors of the GTP-driven FtsZ polymerization and its associated GTPase activity.

Inhibitory Potencies of GTP Analogs Reflect Their Binding Affinities to FtsZ

Further insight into the molecular mode of action of the GTP analogs was obtained from their binding affinities to FtsZ (Table 1), which were determined by a fluorescent competition assay with 2'/3'-O-(*N*-methyl-anthraniloyl)-guanosine-5'-triphosphate (mantGTP), as previously described (Huecas et al., 2007). To this end, stable, nucleotide-free FtsZ from *Methanococcus janaschii* was employed, since apo-FtsZ from *E. coli* is unstable.

As illustrated in Figure 2E, both $\log \text{IC}_{50}$ (polymerization) and $\log \text{IC}_{50}$ (GTPase) linearly correlate with $\log K_d$, indicating that the inhibitory potencies of the GTP analogs on FtsZ function are linked to their binding affinities to the FtsZ monomers. In addition, both the binding affinities and the inhibitory potencies of the GTP analogs appear to be roughly related to the minimal sterical requirement of their C8-substituents, which, for nonspherical substituents, are most conveniently described by their respective

a more *syn*-dominated conformational equilibrium in solution. It remains difficult, however, to estimate the energetic relevance of the *syn-anti* conformational equilibrium as compared to numerous other contributions, such as Mg^{2+} -chelation effects and protein-ligand interactions.

The above data indicate that the inhibitory potencies of the GTP analogs on FtsZ function are governed by their binding affinities to the FtsZ monomers, with increasing monomer binding affinities resulting in more potent inhibition of both FtsZ polymerization and the associated GTPase activity.

Crystal Structure of FtsZ/MorphGTP Reveals Similar Binding Mode of C8-Substituted GTPs and GDP

Up to now, crystallization of functionally active FtsZ in the presence of GTP or analogs containing a nonmodified triphosphate chain has been hampered by the fact that polymerization rates are much faster than crystal growth rates. Our C8-substituted GTP analogs, which, to our knowledge, are the first reported GTP-derived FtsZ inhibitors incorporating the triphosphate moiety, circumvent these problems and stimulated us to attempt crystallization of FtsZ in the presence of the analogs. Our efforts were successful, and resulted in determination of the structure of MorphGTP bound to a truncated construct of *Aquifex aeolicus* FtsZ with 37 residues deleted from the C terminus (AaFtsZΔ37). This construct had previously been used to obtain GDP-containing crystals of high diffraction quality (Oliva et al., 2007). The co-crystals of the MorphGTP-AaFtsZΔ37 complex yielded diffraction

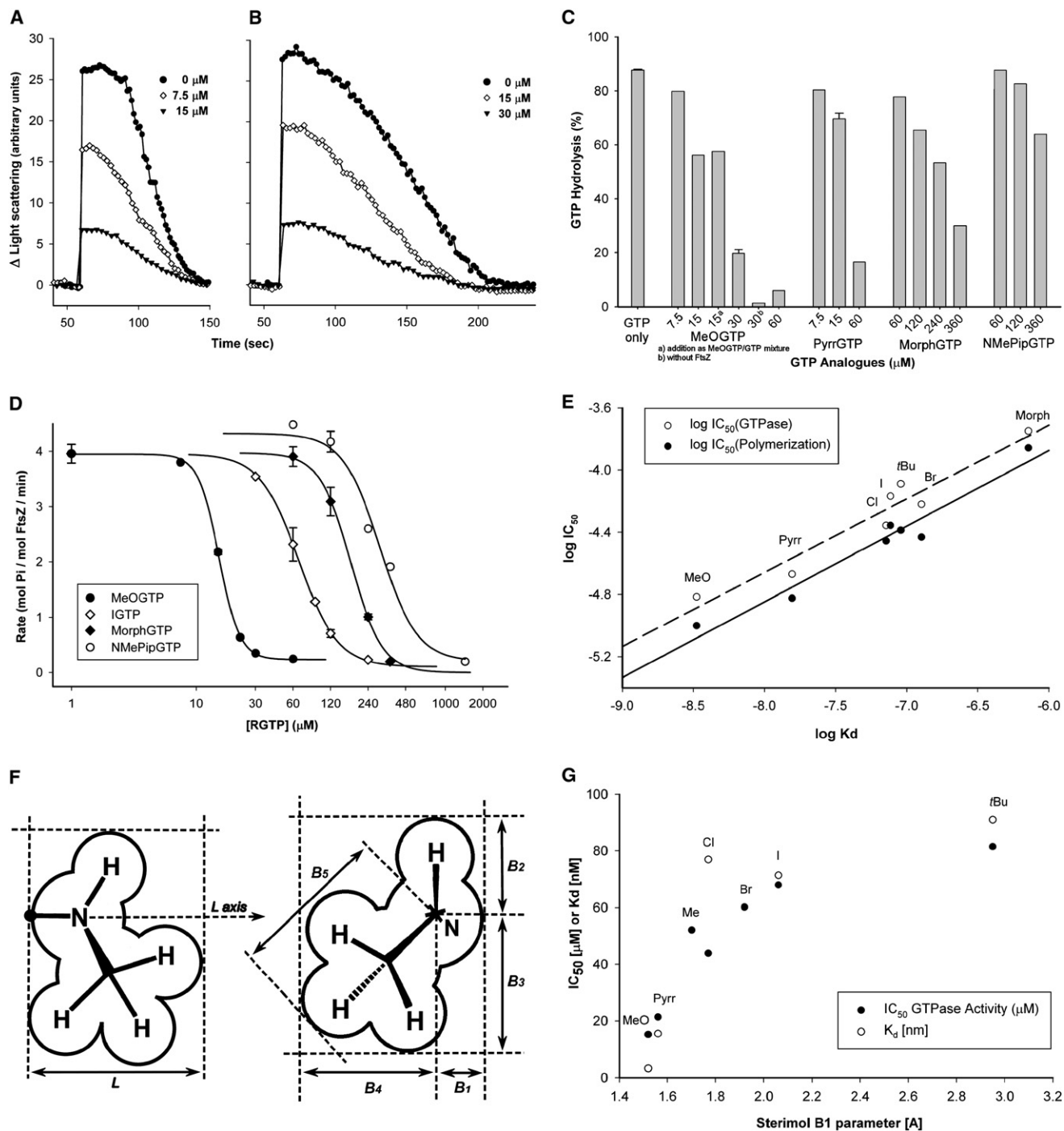


Figure 2. Functional Inhibition of FtsZ by C8-substituted GTP Analogs and Correlation of Inhibitory Potencies with Binding Affinities and Steric Parameters of CC8-Substituents

(A and B) Effect of MeOGTP on FtsZ polymerization measured by 90° angle light scattering. FtsZ (9 μM) was preincubated for 1 min with different concentrations of MeOGTP in 50 mM HEPES/NaOH (pH 7.5), supplemented with 50 mM KCl and 5 mM MgCl₂ at 37°C, and the assay was started by addition of (A) 60 μM GTP or (B) 120 μM GTP.

(C) Inhibition of FtsZ-catalyzed GTP hydrolysis by the two most potent analogs (MeOGTP and PyrrGTP) and the two least potent analogs (MorphGTP and NMePipGTP). After performing the polymerization assays illustrated in (A) (60 μM GTP, t = 150 s), aliquots of the assay mixtures were frozen in liquid nitrogen and the nucleotide composition was analyzed later by reverse-phase HPLC. Error bars represent 1 SD. See Tables S1–S9 for the complete data with all GTP analogs.

(D) Selected log dose–response curves for the inhibition of FtsZ GTPase activity by several GTP analogs. Solid symbols represent measured GTPase activities, and error bars represent ±1 SD. Calculated regression curves are depicted as solid lines. IC₅₀ values were calculated by nonlinear regression analysis. The measurements were performed as described in (A), but assay mixtures also contained 120 μM 7-methylguanosine and 0.3 U/ml nucleoside phosphorylase.

(E) Correlation of log IC₅₀(polymerization) and log IC₅₀(GTPase) with log K_d.

data to a resolution of 1.4 Å, thus providing the highest-resolution FtsZ structure currently available (Table 2). Consistent with previous findings on the structure of FtsZ in different nucleotide states (Oliva et al., 2007), MorphGTP does not seem to induce any significant conformational changes in AaFtsZ relative to its GDP-bound form (Figure 3A).

Electron density maps show clear density for MorphGTP (Figure 3B). The position and conformation of the inhibitor are closely similar to those of the nucleotide in the GDP-containing structure (Oliva et al., 2007), and the morpholino ring forms an angle of approximately 55° with the plane of the guanine base. Although the predominant conformation of the morpholino ring may be clearly discerned, the electron density for this portion of the inhibitor is noticeably weaker than for the base, sugar, and phosphate portions of the molecule. This indicates that the morpholino moiety shows some flexibility, due to the fact that the only direct interaction between the protein and this portion of the inhibitor is a van der Waals contact between a methylene group of the morpholino ring and Phe175, a residue that also forms an important π -stacking contact with the guanine base and is highly conserved in FtsZ homologs from different species.

In conclusion, the diffraction data of the FtsZ/MorphGTP crystals suggests that C8-substituted nucleotides bind to FtsZ in essentially the same way as GTP, explaining their competitive action on GTP-driven FtsZ polymerization.

GTP Analogs with Small C8-Substituents Potentially Promote Tubulin Polymerization

Having classified all C8-substituted GTP analogs (RGTPs) as inhibitors of FtsZ, we set out to characterize their effect on its ortholog, tubulin. Uncovering structural differences in the nucleotide binding sites and intersubunit interactions between these two GTPases could be crucial for designing FtsZ inhibitors, which are nontoxic for eukaryotic cells. First, the structurally diverse RGTPs were probed for their effect on tubulin assembly, employing a common turbidity assay. Surprisingly, some of the RGTPs promoted tubulin assembly more strongly than did GTP itself (Figure 4A), while others showed substantially less or no visible assembly in the same assay under identical conditions (Figure 4B). Examination of the plots obtained with the assembly-promoting RGTP (Figure 4A) shows that the assembly-promoting effects include a reduced lag time before assembly, a steeper slope, and a higher final level of turbidity. Starting from the natural ligand GTP, which is the least potent of the series in Figure 4A, the above three properties increase/decrease in a parallel fashion in the series GTP < IGTP < MeOGTP < BrGTP < CIGTP, with CIGTP displaying about a 2.5-fold higher plateau level of turbidity, a 3.5-fold shorter lag time, and a 5.5-fold shorter $t_{1/2}$ when compared with GTP (Table S10 and Figure S2). After reaching the maximum turbidity, all plots show a gradual decrease. This phenomenon is known for the GTP-dependent polymerization and reflects the

dynamic nature of the polymers, which is powered by continuous nucleotide hydrolysis.

To exclude the possibility that the observed increase in turbidity is simply due to unspecific aggregation, we also tested the cold-reversibility of polymerization. Except for polymers formed in the presence of CIGTP, for which turbidity readings were still 13% of the maximum value after 30 min on ice, the RGTP-induced tubulin polymerization was completely reversible. Upon warming to 37°C, an additional cycle of polymerization could be induced (data not shown). The ability of the GTP analogs to induce the complete sequence of assembly-disassembly-reassembly strongly suggests that the polymers involved are functionally active microtubules.

This conclusion was further confirmed by direct visualization of the polymers by immunofluorescence staining and fluorescence microscopy. Typical images of the polymers formed in the presence of GTP and the assembly-promoting RGTPs are shown in Figure 4C. The shape of the polymers formed in the presence of the RGTPs was indistinguishable from the typical microtubules obtained in the presence of GTP, although the analog-induced polymer network appeared to be more dense and the mean length of the microtubules was apparently reduced. This is perfectly in line with the shorter lag times and $t_{1/2}$ values for the RGTP-induced tubulin assembly observed in the turbidity assay, which, together, point toward enhanced nucleation.

C8-Substituted GTP Analogs Are Substrates of Tubulin GTPase

To determine whether the RGTPs were substrates of the tubulin GTPase function, we determined the nucleotide composition of the assay mixtures after performing the assembly studies described in Figures 4A and 4B. Apart from NMePipGTP, all RGTPs were hydrolyzed. Hydrolysis was generally between 25% and 35%, which is about 15% lower than that observed with the natural substrate GTP (Figure S3). Interestingly, the susceptibility of the RGTPs to tubulin-catalyzed hydrolysis did not seem to be directly related to their potency in the tubulin assembly assays. Uncoupling of tubulin assembly and nucleotide hydrolysis, although unexpected at first sight, has been reported previously (Hamel et al., 1984). Similarly, the C8-substituted GTP analogs described in this study might be substrates of a basal GTPase activity of tubulin.

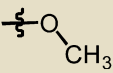
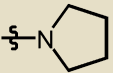
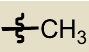
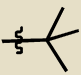
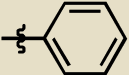
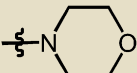
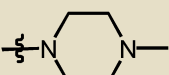
GTP Analogs Compete with GTP for Tubulin Binding and Tubulin-Catalyzed Nucleotide Hydrolysis

To further elucidate their mode of action, we asked ourselves if the GTP analogs could compete with GTP for tubulin binding and tubulin-catalyzed nucleotide hydrolysis. To answer this question, we studied tubulin assembly and tubulin-catalyzed nucleotide hydrolysis in the presence of both the GTP analogs and the natural ligand GTP. We found that the strongly

(F) Illustration of the Sterimol parameters for an arbitrary substituent. Left: perpendicular view on the L axis directed along the bond between the point of attachment on the parent molecule (black dot) and the nitrogen atom of the substituent. Right: view of the same substituent along the L axis (shown as cross). L is the length that the substituent extends along the axis formed by the bond between the substituent and the atom to which it is attached. B1–B4 represent a set of width values perpendicular to both L and to each other, with B1 being the smallest width. B5 represents the longest possible radius perpendicular to L, and forms a good measure of the space required around the L axis in the case of free rotation about the bond connecting the substituent with the parent molecule.

(G) Correlation between the K_d and IC_{50} values of the GTP analogs with the Sterimol B1 parameters of their CC8-substituents. Not included are the considerably less potent MorphGTP and NMePipGTP. Their conformational equilibrium, binding affinities, and inhibitory potencies may primarily be determined by factors other than sterical.

Table 1. Binding Affinities of the GTP Analogues and Functional Inhibition of FtsZ

Nucleotide	R (Substituent at C-8)		Sterimol Parameters ^a	K _{d,app} (nM) ^b	IC ₅₀ Polymerization (μM) ^c	IC ₅₀ GTPase (μM) ^c	GTP Hydrolysis (%) ^d
	Structure of R						
GTP	H		B1: 1.00	3.03 ± 0.93	—	—	90.8 ± 3.4
			B5: 1.00	—	—	—	—
			L: 2.10	—	—	—	—
MeOGTP (6b)			B1: 1.52	3.33 ± 0.65	10	15.3 ± 0.4	5.9
			B5: 3.21	—	—	—	—
			L: 4.24	—	—	—	—
PyrrGTP (7b)			B1: 1.56	15.6 ± 5.7	15	21.4 ± 0.9	16.6
			B5: 3.32	—	—	—	—
			L: 5.38	—	—	—	—
ClGTP (4b)	Cl		B1: 1.77	77 ± 58	35	44.0 ± 3.4	44.2 ± 0.7
			B5: 1.77	—	—	—	—
			L: 3.48	—	—	—	—
MeGTP (1b)			B1: 1.70	—	44	52.0 ± 5.7	Not available
			B5: 2.22	—	—	—	—
			L: 3.08	—	—	—	—
BrGTP (5b)	Br		B1: 1.92	126 ± 38	37 ^e	60.2 ± 8.8 ^e	59.0 ^e
			B5: 1.92	—	—	—	—
			L: 3.79	—	—	—	—
IGTP (3b)	I		B1: 2.06	71 ± 16	44	68.0 ± 4.5	63.8
			B5: 2.06	—	—	—	—
			L: 4.13	—	—	—	—
tBuGTP (2b)			B1: 2.95	91 ± 38	41	81.5 ± 2.9	66.0 ± 1.7
			B5: 3.37	—	—	—	—
			L: 4.34	—	—	—	—
PhGTP (10b)			B1: 1.77	—	71	Not available ^f	72.0
			B5: 3.18	—	—	—	—
			L: 6.28	—	—	—	—
MorphGTP (8b)			B1: 1.78	714 ± 51	139	179 ± 15	77.9
			B5: 3.43	—	—	—	—
			L: 5.51	—	—	—	—
NMePipGTP (9b)			B1: 1.81	—	252	298 ± 33	87.7
			B5: 3.48	—	—	—	—
			L: 7.07	—	—	—	—

The B1 parameter data is set in bold to highlight the fact that they represent the minimal sterical requirement of a C8-substituent.

^a Values are given in Å. The concept of Sterimol parameters is comprehensively described in the legend for Figure 2F.

^b The binding affinity of each ligand was determined by a fluorescent competition assay with mantGTP, employing nucleotide-free FtsZ from *Methanococcus jannaschii* as a model. The equilibrium dissociation constants are from a minimum of two independent displacement curves with each nucleotide. Data reported are mean ± SEM.

^c IC₅₀ values for FtsZ polymerization and GTPase activity were obtained as described in the legend for Figure 2. Data reported are mean ± SEM.

^d Endpoint GTP hydrolysis data are based on the nucleotide composition of the assay mixtures after the polymerization experiments and were determined as described in the legend for Figure 2C. The data reported in this table refer to competition experiments with a 1:1 molar ratio of GTP analog and GTP (both 60 μM). For the complete set of values, see Tables S1–S9.

^e Data obtained under different experimental conditions. HPLC studies were conducted after 300 s instead of 90 s for all other assays. Values reproduced from Lämpchen et al. (2005).

^f GTPase activity cannot be determined with the fluorescent assay due to intensive autofluorescence of PhGTP.

assembly-promoting GTP analogs, when mixed with GTP, were less effective in inducing tubulin assembly than the RGTPs alone (Figure S4). The surprising result, that ClGTP, BrGTP, and IGTP,

which strongly induced tubulin polymerization on their own, were noncumulative with GTP, may suggest that GTP/tubulin and RGTP/tubulin formed two separate pools that did not

copolymerize into the same microtubules. Alternatively, “hybrid” microtubules formed from GTP-charged and RGTP-charged tubulin heterodimers may be intrinsically less stable due to lateral contact instability.

Although many investigations have addressed the effect of GTP analogs on tubulin assembly, most of these earlier studies involved ribose-modified (Hamel et al., 1984) or phosphate-modified nonhydrolyzable analogs (Mejillano et al., 1990). A notable exception is a report on the effects of a series of base-modified purine nucleotides on tubulin polymerization (Muraoka et al., 1999; Muraoka and Sakai, 1999). Two of these nucleotides were actually C8-substituted GTP analogs: the cyclic 2'-deoxy-8,2'-S-GTP with a fixed high-*anti* conformation, and 8-Br-GTP (here referred to as BrGTP). While 2'-deoxy-8,2'-S-GTP did not support assembly, BrGTP was reported to be slightly more effective in promoting polymerization than was GTP itself (Muraoka et al., 1999). This result is in agreement with our present findings, although, in the above investigation, a solution of tubulin containing other, nontubulin proteins was used instead of purified tubulin. Several lines of experimental evidence obtained with the 8-halo-GTPs and MeOGTP strongly suggest competitive binding of these analogs to the β -tubulin E site. First, all RGTPs were found to be hydrolyzed. Second, after performing the tubulin turbidity assay in the presence of assembly-supporting RGTPs only and analogs with equimolar GTP, nucleotide analysis revealed that approximately the same total amount of nucleotide triphosphates was hydrolyzed in both experiments (Figures S3 and S5); that is, GTP hydrolysis in the 8-RGTP/GTP competition assays occurred at the expense of RGTP hydrolysis, and vice versa.

In conclusion, we have shown that GTP analogs with small C8-substituents promote microtubule assembly better than GTP and that all of the C8-substituted GTP analogs are substrates of the tubulin GTPase, strongly suggesting that, similar to FtsZ, 8-RGTPs compete with GTP for binding to the exchangeable nucleotide binding site of tubulin (E site).

Molecular Basis for the Differential Effects of GTP Analogs on FtsZ and Tubulin

Despite the high sequence homology of FtsZ and tubulin found in regions involved in nucleotide binding and the similar protein folds and GTP binding interactions revealed by their crystal structures (Nogales et al., 1998), their active sites formed by association of FtsZ monomers and α , β -tubulin heterodimers appear to be strikingly different. In FtsZ, the nucleotide binding site is more open and partially water filled, allowing free exchange of nucleotides in intact polymers, while in tubulin polymers, the nucleotide is in contact with protein from all sides and is nonexchangeable (Michie and Löwe, 2006; Oliva et al., 2004). As a consequence, in the tubulin active site, nucleotides are confronted with a more hydrophobic environment than in the FtsZ counterpart.

Along these lines, the superior tubulin assembly-promoting effects of the more hydrophobic 8-halo-GTPs compared with GTP may be explained by additional hydrophobic interactions. Apparently, however, with increasing size of the C8-substituents, steric issues become the dominant factor due to space limitations of the nucleotide binding cavity in tubulin. This is reflected in the decreasing potencies in the 8-halo series (CIGTP > BrGTP > IGTP) with increasing van der Waals radius of the halogen (equal

Table 2. Crystallographic Data Collection and Refinement Statistics

Parameters	Values
Space group	P2 ₁
Unit cell parameters a, b, c (Å), β (°)	a = 43.85, b = 74.18, c = 44.20, β = 95.1
Rmsd	
Bond lengths (Å)	0.019
Bond angles (°)	1.843
Resolution range (Å)	20–1.4 (1.5–1.4)
Completeness (%)	94.1 (94.1)
Multiplicity	2.0 (2.0)
$\langle I/\sigma \rangle$	13.4 (4.7)
R _{sym} (%) ^a	5.1 (15.3)
R _{crys} (%) ^b	14.0 (13.6)
R _{free} (%) ^c	18.4 (23.7)

Values in parentheses represent statistics for data in the highest-resolution shell.

^a R_{sym} = $\sum |I - \langle I \rangle| / \sum \langle I \rangle$, where I is a measured intensity and $\langle I \rangle$ is the average intensity from multiple measurements of symmetry-related reflections.

^b R_{crys} = $\sum ||F_o| - |F_c|| / \sum |F_o|$, where $|F_o|$ and $|F_c|$ are the observed and calculated structure factor amplitudes, respectively.

^c R_{free} was calculated by using a random set containing 5% of reflections, which were omitted during refinement.

to its Sterimol B1 parameter), and the dramatically reduced potency of the analogs with larger C8-substituents (PyrrGTP, MorphGTP, PhGTP, and NMePipGTP).

The partially water-filled active site of FtsZ also provides a possible explanation for the GTP analog-induced inhibition of its polymerization, which, according to the currently available protofilament-like structures (Oliva et al., 2004, 2007), may not simply result from direct steric clashes between the C8-substituents of the GTP analogs and the next FtsZ monomer in a growing protofilament. First, even GTP analogs with small C8-substituents may give rise to minor shifts in the protein conformation or induce rearrangement of several water molecules in the active site, leading to a distortion of vital hydrogen bonding interactions required for longitudinal association of subunits. Similarly, even the minor structural changes introduced by the C8-substituents have proven sufficient to affect the binding energetics of the analogs to FtsZ, with the difference of binding free energy change between GTP (the stronger ligand) and MorphGTP being 13.5 kJ/mol. Alternatively, current models of the FtsZ protofilament may not provide a sufficiently accurate description of the true protofilament interface to explain the inhibitory effects of C8-substituted nucleotides. More specifically, it is possible that the present structures of the FtsZ protofilament represent a prehydrolysis conformation (all currently available tubulin structures are post-hydrolysis), and that, after hydrolysis, the two FtsZ monomers move much closer to each other. This could also explain a similar discrepancy noted between the predicted and the observed effects of the W319Y mutant of *M. jannaschii* FtsZ (Oliva et al., 2004). This mutant is unable to polymerize or hydrolyze GTP, despite the fact that it is not involved directly in forming the protofilament interface in any of the current models.

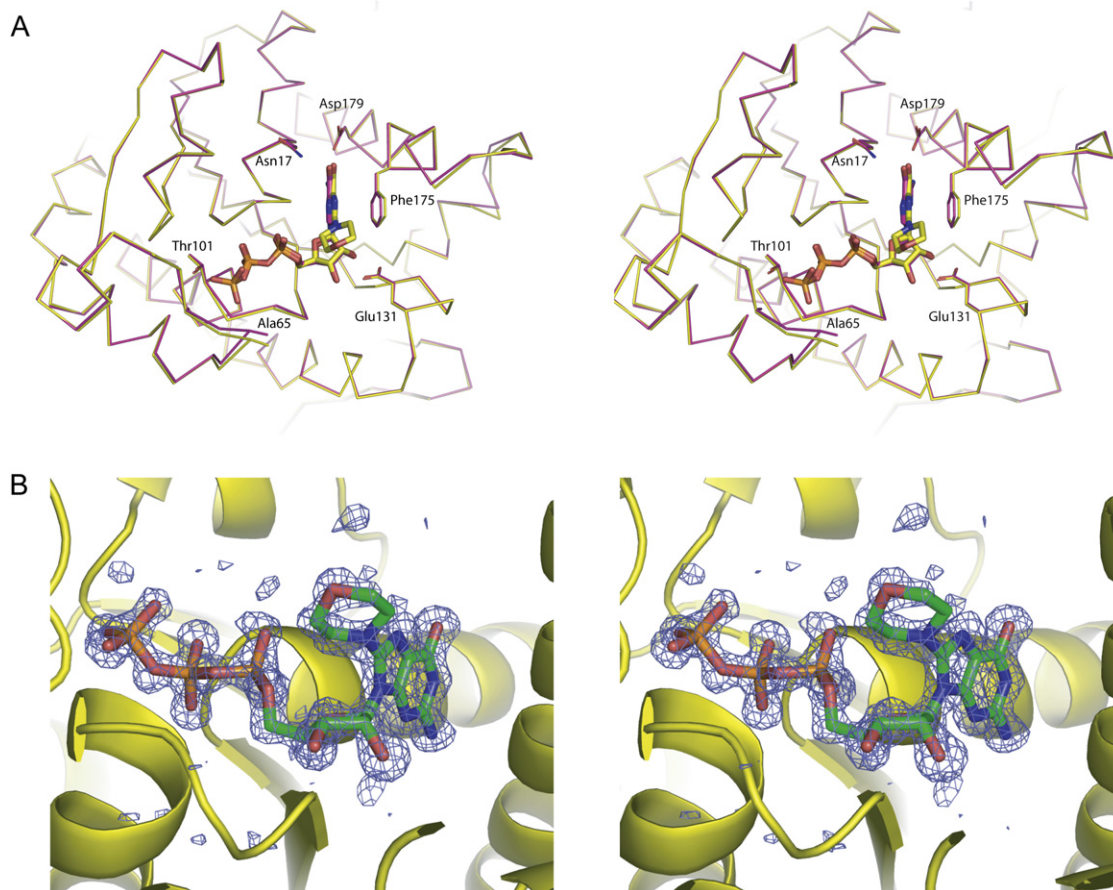


Figure 3. Stereo Views of the Nucleotide Binding Site of *A. aeolicus* FtsZ with Bound MorphGTP

(A) Comparison of AaFtsZ structures bound to MorphGTP (yellow) and GDP (magenta). Side chains of residues that form contacts with MorphGTP are labeled. (B) Electron difference density ($F_o - F_c$) for MorphGTP contoured at 2.5σ .

In summary, our results and those of [Oliva et al. \(2004\)](#) clearly indicate that a more accurate high-resolution model of the FtsZ intersubunit interface in solution would be necessary to resolve the controversy and explain the functional inhibition of FtsZ by C8-substituted GTP analogs.

SIGNIFICANCE

The essential cytoskeletal proteins, FtsZ and tubulin, play a key role in the organization of prokaryotic and eukaryotic cells, respectively. GTP-dependent polymerization of FtsZ into a macromolecular structure called the Z ring is a central event in bacterial cell division, while the microtubules formed upon GTP-induced dynamic assembly of α,β -tubulin heterodimers are indispensable for eukaryotic chromosome segregation. Tubulin and its prokaryotic ortholog, FtsZ, have been extensively studied because of their potential as targets for antiproliferative drugs and antibiotics, respectively. Although a detailed characterization of the intersubunit interfaces in both proteins is of utmost importance for the design of selective modulators of their polymerization dynamics, this issue is still not fully understood.

In contrast to earlier approaches, which mainly relied on crystallographic data or mutational analysis of key residues in the active site located at the intersubunit interface, we sought to elucidate the structural and functional differences in the longitudinal protofilament interfaces of both proteins by using chemically modified analogs of their common ligand GTP. We find that GTP analogs with small hydrophobic substituents at C8 of the nucleobase inhibit FtsZ polymerization efficiently, whereas they stimulate the polymerization of tubulin. Consistent with this result, all of the GTP analogs are resistant to FtsZ-catalyzed hydrolysis and inhibit the polymerization-dependent hydrolysis of GTP. In contrast, GTP analogs stimulating tubulin polymerization are also substrates of its GTPase. The crystal structure of FtsZ in complex with MorphGTP reported in this article illustrates the strength of our ligand modification strategy for active site mapping under biologically relevant conditions, and calls for a re-evaluation of the current models of the FtsZ intersubunit interface. The striking differences in the active sites of FtsZ and tubulin uncovered by our approach should prove crucial for the design of highly selective and potent modulators of their polymerization dynamics.

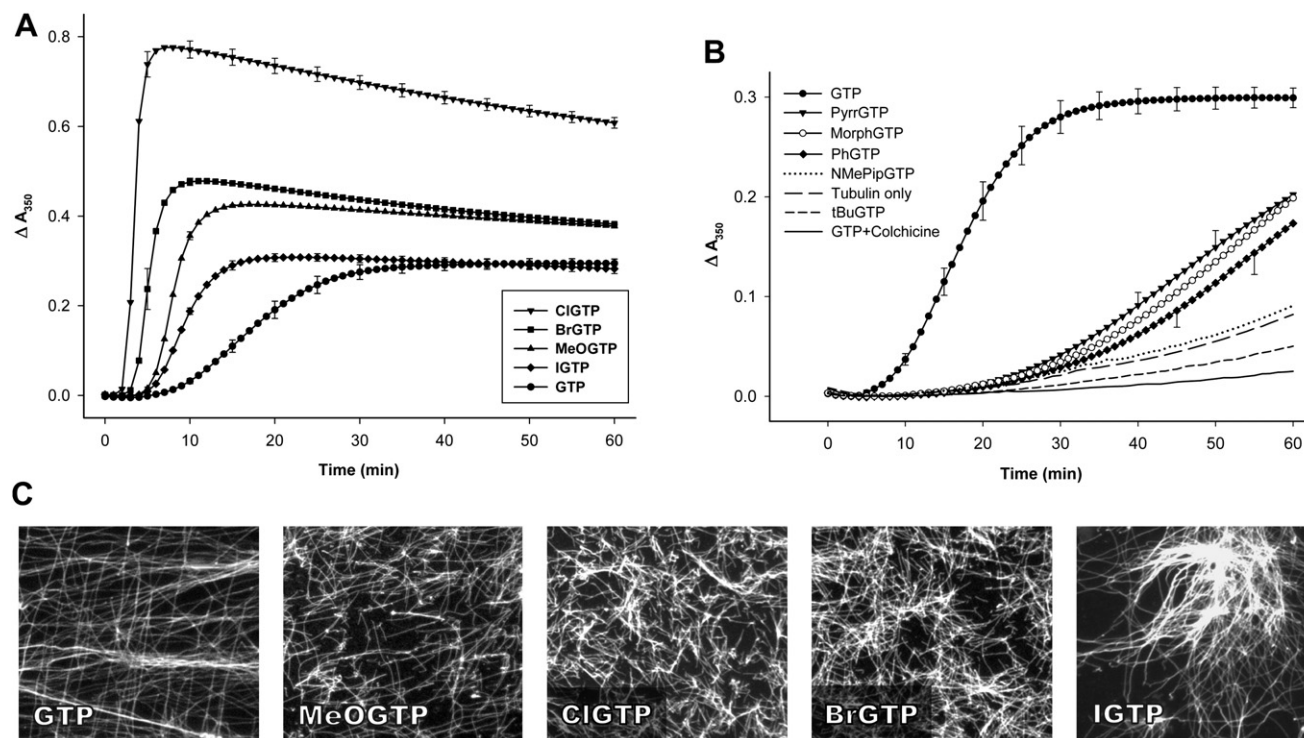


Figure 4. Effect of C8-Substituted GTP Analogs on In Vitro Assembly of Purified Tubulin

(A and B) as monitored by a turbidity assay. (A) GTP analogs, which more potently promote assembly than GTP. (B) GTP analogs, which are less effective than GTP in promoting assembly. Curves are means of duplicate experiments, and error bars represent 1 SD. Briefly, the assay mixtures were prepared on ice in BRB80 buffer (80 mM PIPES/KOH [pH 6.8], 1 mM $MgCl_2$, 1 mM EGTA) and contained 50 μM tubulin and 1.5 mM RGTP or GTP. Just before starting the experiments, the assay mixtures were carefully pipetted to a 96-well plate (duplicate for each nucleotide, 70 μl per well). The plate was transferred to the reader, which was prewarmed to 37°C. A_{350} and the temperature was measured every 30 s for 1 hr.

(C) Fluorescence microscopy images of microtubules formed in the presence of GTP and assembly-promoting GTP analogs, respectively. After the first cycle of assembly described in (A), aliquots of the assay mixtures were processed for immunofluorescence microscopy.

EXPERIMENTAL PROCEDURES

Chemistry

Compounds **1b–10b** were synthesized by following the pathway depicted in Figure 1. Detailed synthetic procedures and spectrometric characterization data are reported in the Supplemental Data.

FtsZ Polymerization and GTPase Studies

Overproduction and Purification of FtsZ

FtsZ was overproduced in *E. coli* BL21(DE3) transformed with pRRE6 and purified as described previously (Scheffers et al., 2000). Protein concentration and purity were determined by amino acid quantification (Eurosequence). FtsZ was 99.4% pure.

Nucleotide Stock Solutions

For the biological tests, we prepared 10 mM stock solutions of the GTP analogs in buffer (50 mM HEPES/NaOH [pH 7.5], 50 mM KCl) with the UV extinction coefficients ϵ of the corresponding nucleosides (see the Supplemental Data). GTP was purchased from Aldrich and a 10 mM GTP stock solution was prepared in the same way with $\epsilon = 13700 M^{-1} cm^{-1}$ ($\lambda_{max} = 253$ nm, pH 7).

Real-Time GTPase Activity and Polymerization Studies

The relatively high absorbance of several GTP analogs at 295 nm (in particular, PhGTP [**10b**] and PyrrGTP [**7b**]) precluded use of the earlier reported combined assay for FtsZ polymerization and GTPase activity (Läppchen et al., 2005). Instead, polymerization was investigated by monitoring light scattering at 350 nm, where the absorbance of all GTP analogs described here was negligible. Regarding the fluorescent assay for phosphate release, the range of acceptable excitation wavelengths for 7-methylguanosine was quite narrow

(290–305 nm), and the inner filter effects of the GTP analogs at these wavelengths needed to be taken into account.

General Procedures. All assays were performed in a stirred quartz cuvette that was maintained at 37°C by a circulating water bath with a PTI QuantaMaster 2000-4 fluorescence spectrophotometer (Photon Technology International). The HEPES buffer (50 mM HEPES/NaOH [pH 7.5], 50 mM KCl) employed in the assay and Millipore water (18.2 M $\Omega \cdot$ cm, used for rinsing the cuvette) were kept at 37°C in a circulating water bath. Stock solutions of nucleoside phosphorylase (10 units/ml), FtsZ (15.7 mg/ml), GTP (10 mM in HEPES buffer), the GTP analogs (10 mM in HEPES buffer), 7-methylguanosine (10 mM in HEPES buffer), and $MgCl_2$ (10 mM in Millipore water) were kept on ice. The cuvette was rinsed with Millipore water. HEPES buffer, $MgCl_2$, and, if appropriate, 7-methylguanosine and nucleoside phosphorylase were added, and the cuvette was allowed to equilibrate in the holder under stirring for 4 min. After the addition of FtsZ, the solution was allowed to equilibrate for 1 min, and air bubbles were manually removed. For the inhibition experiments, the GTP analogs were added and the content of the cuvette was mixed by pipetting. After recording a baseline for 60 s, polymerization was induced by addition of GTP, followed by rapid mixing. The measurement was paused during the addition process, which generally took less than 5 s. Data analysis was performed by nonlinear regression with SigmaPlot V8.02 equipped with Enzyme Kinetics Module V1.1 (SPSS Inc., Chicago, IL).

Polymerization Studies (90° Angle Light Scattering). Both λ (excitation) and λ (emission) were set to 350 nm, and all slit widths were 1.5 nm. The cuvette contained 5 mM $MgCl_2$, 50 mM KCl, 9 μM FtsZ, the GTP analog at the concentration indicated, and 50 mM HEPES/NaOH [pH 7.5], in a total volume of 1.3 ml. After recording a baseline for 60 s, polymerization was induced by addition of

GTP, resulting in a final concentration of 60 μM unless noted otherwise. After 2.5 min, aliquots of the assay mixtures were frozen in liquid nitrogen and the nucleotide composition was determined by ion-exchange (reversed phase) HPLC analysis (see below).

GTPase Activity (Fluorescent Coupled Assay for Phosphate Release). Briefly, phosphate liberated during GTP hydrolysis is a substrate of purine nucleoside phosphorylase, which converts 7-methylguanosine ($\lambda[\text{excitation}] = 302 \text{ nm}$; $\lambda[\text{emission}] = 390 \text{ nm}$) to 7-methylguanine and ribose-1-phosphate, resulting in a decrease of fluorescence. Excitation slit widths were 2 nm and emission slit widths were 6 nm. The cuvette contained 5 mM MgCl_2 , 50 mM KCl, 120 μM 7-methylguanosine, 0.3 U/ml nucleoside phosphorylase, 9 μM FtsZ, the GTP analog at the concentration indicated, and 50 mM HEPES/NaOH [pH 7.5], in a total volume of 1.3 ml. After recording a baseline for 60 s, polymerization was induced by addition of GTP, resulting in a final concentration of 60 μM unless stated otherwise. Standard curves with known phosphate concentrations were used to convert the decrease in fluorescence to phosphate production. In general, the fractional fluorescence change, $(F_0 - F)/F_0$ (where F_0 is initial fluorescence and F is final fluorescence after addition of P_i), was linear up to about 70% of total fluorescence change, indicating that the initial rates may be reliably converted to concentration units. As an additional check, 30 μM KH_2PO_4 was added after termination of the FtsZ-catalyzed reactions (4 min after addition of GTP), and the resulting decrease in fluorescence was recorded.

HPLC Studies

Samples of the assay mixtures (50 μl , see above) were thawed and directly injected into the HPLC system equipped with a Macherey-Nagel CC 125/4 Nucleosil 100-5 C18 HD column (0.4 \times 12.5 cm) and the corresponding guard column and eluted with a linear gradient of buffer A (5 mM $\text{NBu}_4\text{H}_2\text{PO}_4$, 25 mM $\text{H}_3\text{PO}_4/\text{NH}_4\text{OH}$, in 95% water/5% acetonitrile [pH 6.3]) and buffer B (5 mM $\text{NBu}_4\text{H}_2\text{PO}_4$ in 10% water/90% acetonitrile) at 0.4 ml/min flow rate. Gradient details: 0–5 min, 0% B; 5–20 min, 0 \rightarrow 35% B; 20–27 min, 35% B; 27–32 min, 35 \rightarrow 0% B; 32–40 min, 0% B. Detection: UV absorption at the respective λ_{max} of the GTP analogs and at 253 nm (λ_{max} of GTP) with a Pharmacia LKB VWM2141 dual diode array variable wavelength detector. The peaks in the HPLC chromatograms were assigned to specific nucleotide species by comparing the retention times with known standards obtained on the same day (when necessary) and/or by making use of the ratio of the areas of each peak at λ_{max} of the analog and at 253 nm ($A_{\lambda_{\text{max}}}/A_{253}$); that is, peaks with $A_{\lambda_{\text{max}}}/A_{253} > 1$ were identified as GTP analogs and their hydrolysis products. Unfortunately, retention times for the same nucleotide species varied by as much as 2 min for HPLC runs on different days (possibly related to temperature fluctuations). Representative retention times (t_R in minutes) standardized to conditions where GTP results in a retention time of 22.5 min are as follows: GTP (22.5), GDP (18.4); MeOGTP (22.9), MeOGDP (19.1); PyrrGTP (24.0), PyrrGDP (21.4); CiGTP (23.80), CiGDP (20.8); MeGTP (22.5), MeGDP (18.4); BrGTP (23.9) BrGDP (20.9); IGTP (24.0), IGDP (21.1); t-BuGTP (24.6), t-BuGDP (22.4); PhGTP (25.0), PhGDP (22.9); MorphGTP (23.3), MorphGDP (20.0); NMePipGTP (17.4).

Protein Crystallography

AaFtsZ Δ 37 was expressed and purified as previously described (Oliva et al., 2007). Cocrystals with MorphGTP were grown by sitting drop vapor diffusion. Protein/inhibitor mixture (15 g/l AaFtsZ Δ 37, 1.5 mM MorphGTP, 20 mM Tris/HCl [pH 7.5], 1 mM EDTA, 1 mM Na_3N) and reservoir solution (25% PEG400, 60 mM MgCl_2 , 100 mM NaCl) were mixed in equal volumes (500 nl each), and crystals grew to maximum size after 2–3 days. Crystals were frozen in mother liquor with no additional cryoprotectant. Diffraction data were collected to a resolution of 1.4 \AA at ESRF beamline ID23-1 and processed with MOSFLM (Leslie, 1992) and Scala (Evans, 1993). Phases were obtained from the isomorphous structure of GDP-bound AaFtsZ (PDB ID: 2R6R). Initial coordinates and restraint files for MorphGTP were generated with the Dundee PRODRG2 server (Schüttelkopf and van Aalten, 2004), and the structure was refined with Refmac5 (Murshudov et al., 1997).

Tubulin Assembly and GTPase Studies

Preparation of Tubulin

Tubulin was obtained from bovine brain tissue employing two cycles of polymerization-depolymerization in a high-molarity PIPES buffer, as previously described (Castoldi and Popov, 2003). According to SDS-gel electrophoresis,

the tubulin consisting of α,β -heterodimers was > 99% pure and free of microtubule-associated proteins. The tubulin preparation was also free of nucleoside diphosphate kinase activity, since ATP (150 μM) was unable to induce assembly. The total nucleotide content of the tubulin preparation, as determined by HPLC analysis (see below), was about 150 μM (74 μM AMP, 31 μM GDP, 45 μM GTP). The concentration of the final tubulin stock solution in BRB80 buffer (80 mM PIPES/KOH [pH 6.8], 1 mM MgCl_2 , 1 mM EGTA), as determined by its absorbance at 280 nm (A_{280}) with $\epsilon_{280} = 115,000 \text{ M}^{-1} \text{ cm}^{-1}$ (Castoldi and Popov, 2003), was 25 mg/ml (250 μM).

Nucleotide Stock Solutions

For the GTP analogs (RGTPs) and GTP, we employed the 10 mM stock solutions in HEPES buffer prepared as described above for the FtsZ studies.

Turbidity Assay

In vitro tubulin assembly was observed by measuring the change in light scattering at 350 nm (A_{350}). The experiments were carried out in a Spectramax (Molecular Probes) spectrophotometer/plate reader with half-area 96-well plates (CLS3695; Corning). Tests with each nucleotide were performed in triplicate, with a total volume of 70 μl per well. As much as 250 μl of the assay mixtures, sufficient for the triplicates, was prepared on ice. The assay mixtures were prepared in BRB80 buffer and contained 50 μM tubulin and 1.5 mM RGTP or GTP. Just before starting the experiments, the assay mixtures were carefully pipetted to the wells of a precooled well plate to avoid any formation of air bubbles. The plate was transferred to the reader, which was prewarmed to 37°C. A_{350} and the temperature was measured every 30 s for 1 hr. Warming the plate to 37°C took about 2–3 min. To check the reversibility of assembly, and to discriminate the turbidity from an unspecific protein precipitation, the plate was subsequently placed on ice, and turbidity was checked every 10 min for 30 min. The GTP analogs that promoted assembly more than GTP itself were assayed for their ability to induce an additional cycle of assembly by warming the plate to 37°C again and measuring turbidity development for another hour as in the first cycle. Data analysis was performed with Microsoft Office Excel and SigmaPlot V8.02 equipped with Enzyme Kinetics Module V1.1.

Immunofluorescence Staining and Microscopy

After the first cycle of assembly, for GTP and each of the strongly assembly-promoting RGTPs, 20 μl samples from representative wells were carefully added to 1 ml fixation buffer (1% glutaraldehyde and 0.5% Triton X-100 in BRB80 buffer) and centrifuged onto glass coverslips through 5 ml of a 20%–30% glycerol cushion, as previously described (Evans et al., 1985). After post-fixation with methanol at -20°C for 15 min, the coverslips were washed with PBS (3 \times , fast), PBS + NaBH_4 (1 \times 5 min), PBS (2 \times , fast), PBST (PBS + 0.5% Triton) (1 \times 1 min), and incubated for 30 min with a monoclonal mouse anti- α -tubulin antibody (clone DM1A, ascitic fluid; Sigma) 1/200 in PBST. Following additional washings with PBST (3 \times 5 min), the coverslips were incubated for 30 min with a goat anti-mouse-Alexa488 conjugate (A11001 IgG 2 mg/ml; Molecular probes) 1/1000 in PBST and rinsed with PBST (3 \times 5 min). Excess of fluid was carefully removed and the coverslips were mounted on glass slides with Fluorsave Reagent mounting liquid (Calbiochem). For the observation of samples and image acquisitions, we used an Axiovert 200M microscope (Zeiss) coupled with a Coolsnap HQ camera (Roper Scientific), driven by the Metamorph software (Universal Imaging Corporation).

HPLC Studies

After 60 min, aliquots of the turbidity assay mixtures were frozen in liquid nitrogen, and the nucleotide composition was subsequently determined. Samples were thawed, diluted 1:10 with Millipore water, directly injected into the HPLC system, and analyzed as described above for the FtsZ GTPase studies.

ACCESSION NUMBERS

Atomic coordinates of the *Aquifex aeolicus* FtsZ with 8-morpholino-GTP have been deposited in the Protein Data Bank with accession code 2R75.

SUPPLEMENTAL DATA

Supplemental Data, including Tables S1–S10, Figures S1–S5, and full experimental details and spectroscopic data for both the C8-substituted guanosine 5'-triphosphates and the intermediate C8-substituted guanosines, are available online at <http://www.chembiol.com/cgi/content/full/15/2/189/DC1/>.

ACKNOWLEDGMENTS

This work was supported in part by a Netherlands Organization for Scientific Research "Vernieuwingsimpuls" grant (016.001.024, T.d.B.) and grants MEC BFU 2005-00505/BMC and CAM S-BIO-0214-2006 (J.M.A.). A.V.P. acknowledges support by the Avenir grant of Inserm, ACI BCMS of the French Research Ministry (project BCM0210), and equipment grants of the "La Ligue contre le Cancer" (Comité de l'Isère) and the "Association pour la Recherche sur le Cancer" (project 7833). A.J. was funded by the program "Emergence 2004" of the Department of Rhône-Alpes. We would also like to thank Machteld Petram for the synthesis of some of the C8-substituted guanosines and Bart Stegink for carrying out several of the triphosphorylations.

Received: October 31, 2007

Revised: December 21, 2007

Accepted: December 28, 2007

Published: February 22, 2008

REFERENCES

- Castoldi, M., and Popov, A.V. (2003). Purification of brain tubulin through two cycles of polymerization-depolymerization in a high-molarity buffer. *Protein Expr. Purif.* **32**, 83–88.
- Erickson, H.P. (1995). FtsZ, a prokaryotic homolog of tubulin? *Cell* **80**, 367–370.
- Evans, L., Mitchison, T., and Kirschner, M. (1985). Influence of the centrosome on the structure of nucleated microtubules. *J. Cell Biol.* **100**, 1185–1191.
- Evans, P.R. (1993). Data reduction. Proceedings of CCP4 Study Weekend, 1993, on Data Collection & Processing. pp. 114–122.
- Hamel, E., Lustbader, J., and Lin, C.M. (1984). Deoxyguanosine nucleotide analogues: Potent stimulators of microtubule nucleation with reduced affinity for the exchangeable nucleotide site of tubulin. *Biochemistry* **23**, 5314–5325.
- Huang, Q., Kirikae, F., Kirikae, T., Pepe, A., Amin, A., Respicio, L., Slayden, R.A., Tonge, P.J., and Ojima, I. (2006). Targeting FtsZ for antituberculosis drug discovery: noncytotoxic taxanes as novel antituberculosis agents. *J. Med. Chem.* **49**, 463–466.
- Huang, Q., Tonge, P.J., Slayden, R.A., Kirikae, T., and Ojima, I. (2007). FtsZ: a novel target for tuberculosis drug discovery. *Curr. Top. Med. Chem.* **7**, 527–543.
- Huecas, S., and Andreu, J.M. (2003). Energetics of the cooperative assembly of cell division protein FtsZ and the nucleotide hydrolysis switch. *J. Biol. Chem.* **278**, 46146–46154.
- Huecas, S., Schaffner-Barbero, C., Garcia, W., Yebenes, H., Palacios, J.M., Diaz, J.F., Menendez, M., and Andreu, J.M. (2007). The interactions of cell division protein FtsZ with guanine nucleotides. *J. Biol. Chem.* **282**, 37515–37528.
- Läppchen, T., Hartog, A.F., Pinas, V.A., Koomen, G.J., and den Blaauwen, T. (2005). GTP analogue inhibits polymerization and GTPase activity of the bacterial protein FtsZ without affecting its eukaryotic homologue tubulin. *Biochemistry* **44**, 7879–7884.
- Leslie, A.G.W. (1992). Recent changes to the MOSFLM package for processing film and image plate data. Joint CCP4 & ESF-EAMCB Newslett. *Protein Crystallogr.* **26**.
- Lipkin, D., Howard, F.B., Nowotny, D., and Sano, M. (1963). The iodination of nucleosides and nucleotides. *J. Biol. Chem.* **238**, PC2249–PC2251.
- Long, R.A., Robins, R.K., and Townsend, L.B. (1968). 8-Bromoguanosine. In *Synthetic Procedures in Nucleic Acid Chemistry*, W.W. Zorbach, and R.S. Tipson, eds. (New York: Wiley Interscience), pp. 228–229.
- Löwe, J., and Amos, L.A. (1998). Crystal structure of the bacterial cell division protein FtsZ. *Nature* **391**, 203–206.
- Löwe, J., and Amos, L.A. (2000). Helical tubes of FtsZ from *Methanococcus jannaschii*. *Biol. Chem.* **381**, 993–999.
- Löwe, J., Li, H., Downing, K.H., and Nogales, E. (2001). Refined structure of α -tubulin at 3.5 Å resolution. *J. Mol. Biol.* **313**, 1045–1057.
- Lu, C., Reedy, M., and Erickson, H.P. (2000). Straight and curved conformations of FtsZ are regulated by GTP hydrolysis. *J. Bacteriol.* **182**, 164–170.
- Maeda, M., Nushi, K., and Kawazoe, Y. (1974). Studies on chemical alterations of nucleic acids and their components—VII. *Tetrahedron* **30**, 2677–2682.
- Mejillano, M.R., Barton, J.S., Nath, J.P., and Himes, R.H. (1990). GTP analogues interact with the tubulin exchangeable site during assembly and upon binding. *Biochemistry* **29**, 1208–1216.
- Michie, K.A., and Löwe, J. (2006). Dynamic filaments of the bacterial cytoskeleton. *Annu. Rev. Biochem.* **75**, 467–492.
- Mingorance, J., Rueda, S., Gómez-Puertas, P., Valencia, A., and Vicente, M. (2001). *Escherichia coli* FtsZ polymers contain mostly GTP and have a high nucleotide turnover. *Mol. Microbiol.* **41**, 83–91.
- Mukherjee, A., Dai, K., and Lutkenhaus, J. (1993). *Escherichia coli* cell division protein FtsZ is a guanine nucleotide binding protein. *Proc. Natl. Acad. Sci. USA* **90**, 1053–1057.
- Mukherjee, A., and Lutkenhaus, J. (1998). Dynamic assembly of FtsZ regulated by GTP hydrolysis. *EMBO J.* **17**, 462–469.
- Muraoka, M., and Sakai, H. (1999). Effects of purinenucleotide analogues on microtubule assembly. *Cell Struct. Funct.* **24**, 305–312.
- Muraoka, M., Fukuzawa, H., Nishida, A., Okano, K., Tsuchihara, T., Shimoda, A., Suzuki, Y., Sato, M., Osumi, M., and Sakai, H. (1999). The effects of various GTP analogues on microtubule assembly. *Cell Struct. Funct.* **24**, 101–109.
- Murshudov, G.N., Vagin, A.A., and Dodson, E.J. (1997). Refinement of macromolecular structures by the maximum-likelihood method. *Acta Crystallogr. D Biol. Crystallogr.* **53**, 240–255.
- Nogales, E., and Wang, H.W. (2006a). Structural intermediates in microtubule assembly and disassembly: how and why? *Curr. Opin. Cell Biol.* **18**, 179–184.
- Nogales, E., and Wang, H.W. (2006b). Structural mechanisms underlying nucleotide-dependent self-assembly of tubulin and its relatives. *Curr. Opin. Struct. Biol.* **16**, 221–229.
- Nogales, E., Downing, K.H., Amos, L.A., and Löwe, J. (1998). Tubulin and FtsZ form a distinct family of GTPases. *Nat. Struct. Biol.* **5**, 451–458.
- Oliva, M.A., Cordell, S.C., and Löwe, J. (2004). Structural insights into FtsZ protofilament formation. *Nat. Struct. Mol. Biol.* **11**, 1243–1250.
- Oliva, M.A., Trambaiolo, D., and Löwe, J. (2007). Structural insights into the conformational variability of FtsZ. *J. Mol. Biol.* **373**, 1229–1242.
- Paradis-Bleau, C., Beaumont, M., Sanschagrin, F., Voyer, N., and Levesque, R.C. (2007). Parallel solid synthesis of inhibitors of the essential cell division FtsZ enzyme as a new potential class of antibacterials. *Bioorg. Med. Chem.* **15**, 1330–1340.
- Pless, R., Dudycz, L., Stolarski, R., and Shugar, D. (1978). Purine nucleosides and nucleotides unequivocally in the *syn* conformation: guanosine and 5'-GMP with 8-*tert*-butyl and 8-(α -hydroxyisopropyl) substituents. *Z. Naturforsch. [C]* **33c**, 902–907.
- Romberg, L., and Mitchison, T.J. (2004). Rate-limiting guanosine 5'-triphosphate hydrolysis during nucleotide turnover by FtsZ, a prokaryotic tubulin homologue involved in bacterial cell division. *Biochemistry* **43**, 282–288.
- Ryu, E.K., and MacCoss, M. (1981). New procedure for the chlorination of pyrimidine and purine nucleosides. *J. Org. Chem.* **46**, 2819–2823.
- Scheffers, D.-J., den Blaauwen, T., and Driessen, A.J.M. (2000). Non-hydrolysable GTP- γ -S stabilizes the FtsZ polymer in a GDP-bound state. *Mol. Microbiol.* **35**, 1211–1219.
- Scheffers, D.-J., de Wit, J.G., den Blaauwen, T., and Driessen, A.J.M. (2002). GTP hydrolysis of cell division protein FtsZ: evidence that the active site is formed by the association of monomers. *Biochemistry* **41**, 521–529.
- Schüttelkopf, A.W., and van Aalten, D.M.F. (2004). PRODRG—a tool for high-throughput crystallography of protein-ligand complexes. *Acta Crystallogr. D Biol. Crystallogr.* **60**, 1355–1363.
- Vollmer, W. (2006). The prokaryotic cytoskeleton: a putative target for inhibitors and antibiotics? *Appl. Microbiol. Biotechnol.* **73**, 37–47.
- Western, E.C., Daft, J.R., Johnson, E.M., Gannett, P.M., and Shaughnessy, K.H. (2003). Efficient one-step Suzuki arylation of unprotected halonucleosides, using water-soluble palladium catalysts. *J. Org. Chem.* **68**, 6767–6774.